Contribution from the Dipartimento di Scienze Chimiche, University of Catania, 95125 Catania, Italy, Dipartimento di Chimica Inorganica, Metallorganica ed Analitica, University of Padova, 35100 Padova, Italy, Istituto di Chimica, University of Basilicata, 85100 Potenza, Italy, and Department of Chemistry and Materials Research Center, Northwestern University, Evanston, Illinois 60208

Electronic Structure of Tetracoordinate Transition-Metal Complexes. 2.† Comparative Theoretical ab Initio/Hartree–Fock–Slater and UV–Photoelectron Spectroscopic Studies of Building Blocks for Low-Dimensional Conductors: Glyoximate Complexes of Palladium(II) and Platinum(II)‡

Santo Di Bella,[1a] Maurizio Casarin,[1b] Ignazio Fragalà,*[,1a] Gaetano Granozzi,*[,1c] and Tobin J. Marks*[,1d]

Received January 22, 1988

This contribution presents an integrated experimental He I/He II UV photoelectron spectroscopic and theoretical ab initio pseudopotential and first-principles local exchange DV–Xα approach to understanding the electronic structure of the bis(glyoximato) (gly) complexes of Pd(II) and Pt(II). Theoretical results include evaluation of reorganization energies in the ion state to interpret PE spectroscopic data as well as relativistic corrections to account for the effect of the heavy atom in $Pt(gly)_2$. These results provide convincing descriptions of the metal–ligand bonding. The bonding involves almost all of the upper filled molecular orbitals (σ and π) of the ligand cluster. In particular, interactions with orbitals of σ symmetry involve empty nd_{xy} and $(n+1)$s metal orbitals and result in an appreciable ligand-to-metal charge transfer. This effect is especially important in the case of the Pt complexes and raises the energies of metal d subshells. Detailed assignments of the UV PE spectra are proposed on the basis of both theoretical results (ΔSCF and TSIE calculations) and He I/He II intensity changes in the PE spectra. The present results argue that charge transport in low-dimensional, partially oxidized $[Pd(gly)_2^{+\rho}]_n$ systems will occur via bands that are significantly ligand π-electron in character (as in $Ni(Pc)^{+\rho}$ salts). In contrast, transport in the corresponding $[Pt(gly)_2^{+\rho}]_n$ systems is likely to be via a largely metal-based band structure (as in conductive tetracyanoplatinate salts).

Introduction

vic-Dioximes (glyoximes) form complexes with a large variety of transition-metal ions.[2] The properties of these complexes have attracted much attention, and many studies have appeared on their electronic structure,[3] stabilities,[4] and charge-transport properties.[5] X-ray diffraction studies have shown that some glyoximato complexes of d^8 metal ions (Figure 1) possess 1-D crystal structures[6] that, in turn, form electrically conducting systems (10^{-3}–10^{-5} Ω cm^{-1}) upon partial oxidation with halogens.[5]

Within a simple "tight-binding" band structure model,[7] the collective optical, electrical, and magnetic properties of these complexes as well as of those of a large variety of highly conjugated ligands can be described in terms of favorable overlap between frontier orbitals of the stacked units modulated by the particular spatial orientation and chain structure existing in the crystals. In particular, the segregated stacking of the molecular subunits may favor intermolecular interactions involving either metal-based (MB) or ligand-based (LB) orbitals. Nevertheless, molecular orbital (MO) calculations on *vic*-dioximates have been inconclusive since different orderings of MB MO's have been found, and moreover, there are actual doubts as to whether or not one such MB orbital is actually the highest lying occupied MO (HOMO).[3] In this context, it becomes a central issue to understand the details of the electronic structures of the stacked molecular subunits. Integrated studies utilizing He I/He II UV photoelectron spectroscopic (PES) measurements combined with high-quality ab initio and first-principles Hartree–Fock–Slater theoretical calculations probably represent the most powerful tool currently available to obtain such information.[8,9] Therefore, we were prompted to begin the first systematic spectroscopic/quantum-chemical studies of Ni-triad planar complexes that form low-dimensional crystals,[10] and in this paper we report on the electronic structure properties of the glyoximato (gly) and dimethylglyoximato (dmg) complexes of Pd(II) and Pt(II) (Figure 1).

Experimental Section

The complexes of interest were prepared[5] by reaction between $PdCl_2$ (acidified with HCl) or K_2PtCl_4 and an alcoholic solution of glyoxime (Hgly, Fluka) or dimethylglyoxime (Hdmg, Carlo Erba). The products were purified first by recrystallization from chloroform or water and then by sublimation in vacuo. The complexes gave satisfactory mass spectrometric analyses.[4]

PE spectra were recorded on a PS18 Perkin-Elmer spectrometer modified by the inclusion of a hollow cathode discharge source giving a high output of He II photons (Helectros Development Corp.). The spectra were accumulated in the "multiple scan mode" with the aid of an IBM PC XT computer directly interfaced to the spectrometer. The energy scale of consecutive scans were locked to the reference values of the Ar and He $1s^{-1}$ self-ionization lines. The spectra were deconvoluted by fitting the spectral profiles with a series of asymmetric Gaussian curves after subtraction of the background. The areas of bands thus evaluated are considered accurate to ±5% (as derived from the fitting procedure).

Computational Details

Ab initio LCAO–MO–SCF calculations were carried out by using pseudopotentials to simulate all core electrons of each atom. The Durand and Barthelat formalism[11] was chosen. For any atom C, the pseudopo-

† For part 1 see ref 8.

‡ Based on a thesis, submitted by S.D.B. to the Ministero della Pubblica Istruzione (MPI, Rome), in partial fulfillment of the requirements for the Ph.D. degree, Dec 1986.

(1) (a) University of Catania. (b) University of Basilicata. (c) University of Padova. (d) Northwestern University.
(2) Lindoy, L. F.; Livingstone, S. E. *Coord. Chem. Rev.* **1967**, *2*, 173.
(3) (a) Ingraham, L. L. *Acta Chem. Scand.* **1966**, *20*, 283. (b) Ohashi, Y.; Hanazaki, I.; Nagakura, S. *Inorg. Chem.* **1970**, *9*, 2551. (c) De Alti, G.; Galasso, V.; Bigotto, A. *Inorg. Chim. Acta* **1970**, *4*, 267. (d) Attanassov, M. A.; St. Nikolov, G. *Inorg. Chim. Acta* **1983**, *68*, 15. (e) Böhm, M. C. *Theor. Chim. Acta* **1983**, *62*, 373. (f) Böhm, M. C. *Physica B+C (Amsterdam)* **1984**, *124*, 203. (g) Alvarez, S.; Canadell, E. *Solid State Commun.* **1984**, *50*, 141.
(4) Westmore, J. B.; Fung, D. K. C. *Inorg. Chem.* **1983**, *22*, 902.
(5) (a) Miller, J. S. *Inorg. Chem.* **1977**, *16*, 957. (b) Cowie, M.; Gleizes, A.; Grynkewich, G. W.; Kalina, D. W.; McClure, M. S.; Scaringe, R. P.; Teitelbaum, R. C.; Ruby, S. L.; Ibers, J. A.; Kannewurf, C. R.; Marks, T. J. *J. Am. Chem. Soc.* **1979**, *101*, 2921. (c) Brown, L. D.; Kalina, D. W.; McClure, M. S.; Schultz, S.; Ruby, S. L.; Ibers, J. A.; Kannewurf, C. R.; Marks, T. J. *J. Am. Chem. Soc.* **1979**, *101*, 3947. (d) Kalina, D. W.; Lyding, J. W.; Ratajack, M. T.; Kannewurf, C. R.; Marks, T. J. *J. Am. Chem. Soc.* **1980**, *102*, 7854.
(6) (a) Godycki, L. E.; Rundle, R. E. *Acta Crystallogr.* **1953**, *6*, 487. (b) Williams, D. E.; Wohlauer, G.; Rundle, R. E. *J. Am. Chem. Soc.* **1959**, *81*, 755. (c) Frasson, E.; Panattoni, C.; Zannetti, R. *Acta Crystallogr.* **1959**, *89*, 2132.
(7) (a) Miller, J. S.; Epstein, A. J. *Progr. Inorg. Chem.* **1976**, *20*, 1. (b) Devreese, J. T.; Evrard, R. P.; Van Doren, V. E. *Highly Conducting One-Dimensional Solids*, Plenum: New York, 1979. (c) Whangbo, M.-H. In *Crystal Chemistry and Properties of Materials with Quasi-One-Dimensional Structures*; Rouxel, J., Ed., Reidel: Dordrecth, The Netherlands, 1986; p 27. (d) Miller, J. S., Ed. *Extended Linear Chain Compounds*; Plenum: New York: 1982, Vol. 1, 2; 1983, Vol. 3.
(8) Di Bella, S.; Fragalà, I.; Granozzi, G. *Inorg. Chem.* **1986**, *25*, 3997 and references therein.
(9) Casarin, M.; Vittadini, A.; Granozzi, G.; Fragalà, I.; Di Bella, S. *Chem. Phys. Lett.* **1987**, *141*, 193.
(10) Marks, T. J.; Kalina, D. W. In *Extended Linear Chain Compounds*; Miller, J. S., Ed.; Plenum: New York, 1982; Vol. 1, p 197.

0020-1669/88/1327-3993$01.50/0

Table I. PSHONDO Eigenvalues and Population Analysis of the Outermost MO's of Hgly

MO	eigenvalue,[a] eV	% pop. N	C	O	H	H′	MO type
			cis-Hgly				
$2a_2$	−9.86 (−9.82)	45	29	26			π_4
$6b_1$	−12.04 (−12.03)	63	5	24	6	2	n_-
$7a_1$	−12.60 (−12.55)	58	7	26	8	1	n_+
$2b_2$	−12.70 (−12.66)	14	45	41			π_3
$6a_1$	−16.19 (−16.13)	6	44	30	9	11	σ
$1a_2$	−16.27 (−16.22)	23	5	72			π_2
$1b_2$	−16.75 (−16.70)	29	17	54			π_1
$5b_1$	−17.07 (−17.03)	17	24	39	18	2	σ
			trans-Hgly				
$2b_g$	−10.05 (−10.00)	46	27	27			π_4
$7a_g$	−12.49 (−12.44)	58	7	24	10	1	n_+
$6b_u$	−12.54 (−12.52)	62	6	26	4	2	n_-
$2a_u$	−12.82 (−12.76)	14	44	42			π_3
$6a_g$	−16.18 (−16.12)	2	45	29	14	10	σ
$1b_g$	−16.41 (−16.36)	24	4	72			π_2
$1a_u$	−16.88 (−16.83)	30	17	53			π_1
$5b_u$	−18.00 (−17.99)	16	12	56	7	9	σ

		N	C	O	H	H′
orbital pop.[b]	s	1.665 (1.663)	1.197 (1.201)	1.872 (1.870)	0.830 (0.848)	0.650 (0.650)
	p_σ	2.244 (2.227)	1.882 (1.872)	2.660 (2.670)		
	p_π	1.143 (1.107)	0.917 (0.955)	1.940 (1.937)		
atomic charges[b]		−0.052 (+0.003)	+0.004 (−0.028)	−0.472 (−0.477)	+0.170 (+0.152)	+0.350 (+0.350)

		N–C	C–C	N–O	C–H	O–H′
overlap pop.	σ	0.520 (0.596)	0.584 (0.508)	0.194 (0.176)	0.786 (0.808)	0.542 (0.544)
	π	0.474 (0.484)	0.020 (−0.014)	−0.044 (−0.016)		

[a] GAUSSIAN 80 eigenvalues are reported in parentheses. [b] Values for the cis conformer are reported in parentheses.

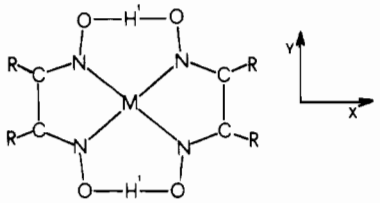

Figure 1. Geometry of square-planar glyoximato complexes.

tential is expressed through the local operator for each l value as in eq 1. Literature values of a_i, $n(i)$ and α parameters have been used.[12] In

$$W_{l,c}(r) = \sum_i a_i r^{n(i)} \exp(-\alpha r^2) \quad (1)$$

the case of the Pt atom, the pseudopotentials[13] include the major (mass and Darwin) relativistic corrections.[14] Gaussian basis sets[8] have been optimized for each valence shell by a pseudopotential version of the ATOM program.[15] The standard Huzinaga[16] basis sets have been used for hydrogen atoms. The basis sets have been contracted to double-ζ forms (3+2 for nd and 3+1 components for ns and np atomic orbitals). Calculations have been carried out by using the PSHONDO program[17] (a modified version of the HONDO program,[18] including pseudopotential) on a VAX-11/750 computer. In the case of the Hgly molecule, additional calculations were performed with the GAUSSIAN 80 program[19] and 4-31G standard basis sets.[20] Gross atomic charges and bond overlap populations have been obtained by Mulliken population analyses.[21] Ionization energies (IE's) have been corrected for repolarization and correlation terms upon ionization by using a first-order perturbative treatment (PT).[22] This procedure, although less rigorous than ΔSCF calculations (which, however, neglect the correlation term), requires less computational effort because only one SCF iteration is required to compute each IE value. Furthermore, selected PT IE's have been compared to values obtained by evaluating repolarization energies associated with production of the corresponding ion states using more rigorous ΔSCF calculations, in which the Nesbet operator[23] is used to solve the open-shell problem. ΔSCF IE's are generally comparable to those obtained from the PT (Tables VI and VIII) using a 0.75 factor to scale the PT repolarization energies.[8]

Table II. Relevant PE Data, Computed IE's, and Assignments of the PE Spectra of Hgly and Hdmg

band label	Hgly IE, eV exptl	ΔSCF	PT[a]	rel intens[b] He I	He II	Hdmg IE, eV exptl	assignt
a	9.70	9.34	9.62 (9.35)	1.00	1.00	9.24	π_4 ($2b_g$)
b	10.91	11.71	1.67 (10.84)	1.68	1.78		n_- ($6b_u$)
		11.77	11.78 (11.65)			10.60	n_+ ($7a_g$)
							π_3 ($2a_u$)
c	11.58	12.22	12.28 (12.16)	1.02	1.03		

[a] Values for the cis conformer are reported in parentheses. [b] The intensity of band a has been taken as reference.

First-principles Hartree–Fock–Slater calculations[24,25] were performed with a VAX-11/780 computer. Numerical atomic orbitals (AO's) ob-

(11) (a) Durand, Ph.; Barthelat, J. C. *Theor. Chim. Acta* **1975**, *38*, 283. (b) Barthelat, J. C.; Durand, Ph.; Serafini, A. *Mol. Phys.* **1977**, *33*, 159. (c) Pélissier, M.; Durand, Ph. *Theor. Chim. Acta* **1980**, *55*, 43.
(12) (a) Ortega-Blake, I.; Barthelat, J. C.; Costes-Puech, E.; Oliveros, E. *J. Chem. Phys.* **1982**, *76*, 4130. (b) Daudey, J. P.; Jeung, G.; Ruiz, M. E.; Novaro, D. *Mol. Phys.* **1982**, *46*, 67.
(13) Daudey, J. P., private communication.
(14) Barthelat, J. C.; Pélissier, M.; Durand, Ph. *Phys. Rev. A* **1980**, *21*, 1773.
(15) Dupuis, M.; Rys, J.; King, H. F. "HONDO 76"; *QCPE*, programs 336 and 338; Indiana University, Bloomington, IN.
(16) Huzinaga, S. *J. Chem. Phys.* **1965**, *42*, 1233.
(17) Daudey, J. P., private communication.
(18) Dupuis, M.; Rys, J.; King, H. F. *J. Chem. Phys.* **1976**, *65*, 111.
(19) Chandra, M.; Kollman, P.; Binkley, J. S.; Whiteside, R. A.; Krishnan, R.; Seeger, R.; De Frees, D. J.; Schlegel, H. B.; Topiol, S.; Kahn, L. R.; Pople, J. A. *QCPE*, program 446.
(20) Hehre, W. J.; Stewart, R. F.; Pople, J. A. *J. Chem. Phys.* **1969**, *51*, 2653.
(21) Mulliken, R. S. *J. Chem. Phys.* **1955**, *23*, 1833.
(22) (a) Trinquier, G. *J. Am. Chem. Soc.* **1982**, *104*, 6969. (b) Gonbeau, D.; Pfister-Guillouzo, G. *J. Electron Spectrosc. Relat. Phenom.* **1984**, *33*, 279. (c) Zangrande, G.; Granozzi, G.; Casarin, M.; Daudey, J. P.; Minniti, D. *Inorg. Chem.* **1986**, *25*, 2872.
(23) (a) Nesbet, R. K. *Proc. R. Soc. London, A* **1955**, *230*, 312. (b) Nesbet, R. K. *Adv. Chem. Phys.* **1965**, *9*, 321.
(24) (a) Averill, F. W.; Ellis, D. E. *J. Chem. Phys.* **1973**, *59*, 6412. (b) Rosen, A.; Ellis, D. E.; Adachi, H.; Averill, F. W. *J. Chem. Phys.* **1976**, *65*, 3629.
(25) (a) Trogler, W. C.; Ellis, D. E.; Berkowitz, J. *J. Am. Chem. Soc.* **1979**, *101*, 5896. (b) Delley, B.; Ellis, D. E. *J. Chem. Phys.* **1982**, *76*, 1949.

Table III. Population Analysis of the Outermost MO's of the $(gly)_2^{2-}$ Cluster

	% pop.[a]					
MO	N	C	O	H	H′	character
$2a_u$	30 (36)	37 (28)	33 (36)			π_4
$2b_{3g}$	32 (38)	37 (28)	31 (34)			π_4
$6b_{1g}$	50 (50)	3 (4)	42 (42)	5 (4)		n_-
$7b_{3u}$	40 (35)	3 (3)	52 (59)	5 (3)		n_+
$6b_{2u}$	63 (60)	3 (4)	25 (28)	5 (4)	4 (4)	n_-
$2b_{2g}$	3 (7)	42 (40)	55 (53)			π_3
$7a_g$	56 (53)	5 (5)	27 (32)	9 (6)	3 (4)	n_+
$2b_{1u}$	4 (9)	45 (42)	51 (49)			π_3
$6b_{3u}$	24 (29)	17 (18)	50 (44)	9 (9)		σ
$5b_{1g}$	31 (30)	3 (4)	64 (63)	2 (3)		σ
$1a_u$	30 (32)	7 (6)	63 (62)			π_2
$1b_{3g}$	28 (31)	6 (5)	66 (64)			π_2
$1b_{2g}$	34 (38)	29 (22)	37 (40)			π_1
$6a_g$	6 (4)	42 (44)	33 (32)	8 (10)	11 (10)	σ
$1b_{1u}$	33 (37)	25 (19)	42 (44)			π_1
$5b_{2u}$	26 (22)	19 (21)	38 (39)	16 (16)	1 (2)	σ

	N	C	O	H	H′
orbital pop.[a] s	1.622 (1.573)	1.178 (1.205)	1.928 (1.958)	1.009 (0.834)	0.538 (0.540)
orbital pop.[a] p_σ	2.317 (2.218)	1.784 (1.827)	2.893 (2.615)		
orbital pop.[a] p_π	0.968 (1.144)	1.153 (0.954)	1.879 (1.902)		
atomic charges[a]	+0.093 (+0.065)	−0.115 (+0.014)	−0.700 (−0.475)	−0.009 (+0.166)	+0.462 (+0.460)

	N–C	C–C	N–O	C–H	O–H′
overlap pop.[a] σ	0.922 (0.512)	0.465 (0.512)	−0.009 (0.094)	0.702 (0.788)	0.318 (0.308)
overlap pop.[a] π	0.236 (0.466)	−0.045 (−0.014)	0.019 (−0.012)		

[a] Values for the $(gly)_2$ cluster are reported in parentheses.

Table IV. PSHONDO Eigenvalues and Population Analysis of Outermost MO's of $Pd(gly)_2$

		% population[a]									
		Pd									
MO	eigenvalue,[a] eV	4d	5s	5p	N	C	O	H	H′	overlap pop, Pd–N	dominant character
$3b_{3g}$	−9.88 (5.75)	4 (8)			30 (19)	26 (28)	40 (45)			−0.018	π_4
$2a_u$	−9.92 (5.68)				28 (18)	23 (23)	49 (59)			0.000	π_4
$7b_{3u}$	−11.44 (6.39)			5 (7)	15 (15)	3 (2)	75 (76)	2		0.050	n_+
$9a_g$	−12.04 (6.49)	43 (60)	16 (14)		21 (18)	1	15 (7)	3 (1)	1	0.046	d_{z^2}, n_+
$3b_{2g}$	−12.13 (7.37)	6			3 (3)	41 (37)	50 (60)			−0.006	π_3
$6b_{1g}$	−12.37 (7.34)	7 (11)			2 (1)	2 (3)	88 (85)	1		0.018	n_-
$2b_{1u}$	−12.60 (7.63)				4 (1)	35 (39)	61 (60)			0.000	π_3
$6b_{2u}$	−12.63 (7.54)			4 (5)	48 (41)	4 (2)	37 (46)	4 (4)	3 (2)	0.044	n_-
$6b_{3u}$	−14.36 (9.37)			3	30 (36)	22 (22)	34 (30)	11 (12)		0.038	σ
$2b_{2g}$	−14.47 (7.76)	66 (79)			4	4 (12)	26 (9)			−0.020	d_{xz}, π_1
$2b_{3g}$	−14.56 (7.59)	66 (76)			4 (1)	2 (1)	28 (22)			−0.018	d_{yz}, π_2
$8a_g$	−14.99 (8.09)	59 (64)	(2)		5 (3)	3 (1)	31 (30)	1	1	−0.008	$d_{x^2-y^2}$, d_{z^2}, σ
$1a_u$	−16.21 (10.48)				45 (64)	7 (7)	48 (29)			0.000	π_2
$7a_g$	−16.72 (9.53)	41 (48)			8 (13)	11 (7)	30 (28)	(3)	10 (1)	0.010	σ, $d_{x^2-y^2}$, d_{z^2}
$6a_g$	−16.78 (11.16)	28 (2)			4 (10)	41 (39)	11 (28)	13 (12)	3 (9)	0.034	σ, $d_{x^2-y^2}$
$5b_{1g}$	−17.12 (11.62)	10 (11)			38 (26)	2 (2)	49 (60)	1 (1)		0.020	σ, d_{xy}
$1b_{3g}$	−17.28 (11.06)	29 (10)			38 (61)	4 (5)	29 (24)			0.034	π_2, d_{yz}
$1b_{1u}$	−17.50 (11.70)			1	47 (56)	24 (30)	28 (14)			0.002	π_1
$1b_{2g}$	−18.12 (11.87)	25 (9)			42 (54)	19 (28)	14 (9)			0.036	π_1, d_{xz}
$5b_{2u}$	−18.13 (11.60)			1 (2)	25 (20)	27 (28)	27 (26)	20 (22)	(2)	0.006	σ

[a] Eigenvalues and atomic character from the multipolar DV–Xα calculation are reported in parentheses.

tained from exact Hartree–Fock–Slater calculations were used as basis functions assuming the Gaspar–Kohn–Sham α value.[26] For Pd and N, AO's through 5d and 3p, respectively, were included. For O and C, a minimal 1s, 2s, 2p basis were used. For H, a 1s wave function was used. Core orbitals (1s, ..., 4p for Pd; 1s for O, N, and C) were frozen and orthogonalized against valence orbitals. The Mulliken[21] scheme was used to compute atomic orbital populations. The molecular Coulomb potential was calculated by using a least-squares fit[25] of the model electron density to the true density. Five radial degrees of freedom were allowed in the expansion of the density, in addition to the radial atomic densities. To evaluate the magnitude of electronic relaxation upon ionization of one electron from the various ground state MO's, IE calculations were carried out by using Slater's transition-state (TS) formalism.[27]

The calculations on the Hgly ligand have been made, for both cis (C_{2v}) and trans (C_{2h}) conformations, by using optimized geometrical parameters of glyoxal monoxime[28] with the C–C distance taken from the crystallographic data.[29] In the case of glyoximate complexes, the geometrical parameters were taken from diffraction data[6,30] assuming D_{2h} symmetry. The calculations have been made for model compounds where the methyl groups have been replaced by hydrogen atoms (Figure 1). Present theoretical results always refer to such model complexes. The coordinate system adopted for the calculations is shown in Figure 1.

Results and Discussion

Glyoxime Ligand. The Hgly molecule and the dimethyl derivative Hdmg possess anti-s-trans planar structures linked in the

(26) (a) Gaspar, R. *Acta Phys. Acad. Sci. Hung.* **1954**, *3*, 263. (b) Kohn, W.; Sham, L. J. *Phys. Rev. A* **1965**, *140*, 1133.
(27) Slater, J. C. *Quantum Theory of Molecules and Solids. The Self-Consistent Field for Molecules and Solids*; McGraw-Hill: New York, 1974; Vol. 4.
(28) Bouma, W. J.; Radom, L. *J. Am. Chem. Soc.* **1979**, *101*, 3487.
(29) Calleri, M.; Ferraris, G.; Viterbo, D. *Acta Crystallogr.* **1966**, *20*, 73.
(30) (a) Calleri, M.; Ferraris, G.; Viterbo, D. *Acta Crystallogr.* **1967**, *22*, 468. (b) Calleri, M.; Ferraris, G.; Viterbo, D. *Inorg. Chim. Acta* **1967**, *1*, 297. (c) Ferraris, G.; Viterbo, D. *Acta Crystallogr., Sect. B: Struct. Crystallogr. Cryst. Chem. B* **1969**, *25*, 2066.

Table V. Atomic Charges and Orbital and Overlap Populations of $Pd(gly)_2$ and $Pt(gly)_2$[a]

$Pd(gly)_2$

		Pd	N	C	O	H	H′
orbital pop.	s	0.426	1.510 (1.573)	1.189 (1.205)	1.958 (1.958)	0.834 (0.834)	0.525 (0.540)
	p_σ	0.438	2.358 (2.218)	1.818 (1.827)	2.701 (2.615)		
	p_π	0.012	1.220 (1.144)	0.930 (0.954)	1.866 (1.902)		
	d_σ x^2-y^2	1.948					
	d_σ z^2	1.919					
	d_σ xy	0.746					
	d_π xz	1.945					
	d_π yz	1.980					
atomic charges		+0.586	−0.088 (+0.065)	+0.063 (+0.014)	−0.525 (−0.475)	+0.166 (+0.166)	+0.475 (+0.460)

		Pd–N	N–O	N–C	C–C	C–H	O–H′
overlap pop.	σ	0.501	−0.068 (0.094)	0.382 (0.512)	0.554 (0.512)	0.764 (0.788)	0.304 (0.308)
	π	0.010	0.004 (−0.012)	0.444 (0.466)	0.018 (−0.014)		

$Pt(gly)_2$

		Pt	N	C	O	H	H′
orbital pop.	s	0.993	1.457 (1.573)	1.186 (1.205)	1.965 (1.958)	0.820 (0.834)	0.515 (0.540)
	π_σ	0.104	2.424 (2.218)	1.775 (1.827)	2.673 (2.615)		
	p_π	0.014	1.245 (1.144)	0.921 (0.954)	1.866 (1.902)		
	d_σ x^2-y^2	1.957					
	d_σ z^2	1.888					
	d_σ xy	0.828					
	d_π xz	1.895					
	d_π yz	1.963					
atomic charges		+0.358	−0.126 (+0.065)	+0.118 (+0.014)	−0.504 (−0.475)	+0.180 (+0.166)	+0.485 (+0.460)

		Pt–N	N–O	N–C	C–C	C–H	O–H′
overlap pop.	σ	0.374	−0.050 (0.094)	0.216 (0.512)	0.574 (0.512)	0.808 (0.788)	0.308 (0.308)
	π	−0.010	−0.010 (−0.012)	0.482 (0.466)	0.038 (−0.014)		

[a] Values for the $(gly)_2$ cluster are reported in parentheses.

Table VI. Relevant PE Data, Computed IE's, and Assignments of the PE Spectra of $Pd(gly)_2$ and $Pd(dmg)_2$

band label	$Pd(gly)_2$ IE, eV exptl	ΔSCF[a]	PT[a]	TSIE	$Pd(dmg)_2$ rel intens[c] exptl[b]	He I	He II	assignt[a]
a	8.65	9.50 (0.38)	9.69 (0.34)	8.27	8.00	2.00	2.00	$3b_{3g}$
		9.53 (0.39)	9.72 (0.34)	8.24				$2a_u$
a′		10.50 (1.54)	10.47 (1.68)	9.64	8.30	0.75	1.05	$9a_g$
b	9.56	10.67 (0.77)	10.80 (0.73)	9.05	8.99	0.80	0.90	$7b_{3u}$
c	10.23	11.48 (0.89)	11.59 (0.89)	10.06	9.47	0.67	0.66	$6b_{1g}$
c′		12.51 (1.96)	12.44 (2.10)	11.26	9.64	0.67	1.07	$2b_{2g}$
d	10.72	12.56 (2.00)	12.41 (2.22)	11.04	10.07	1.60	1.85	$2b_{3g}$
		11.79 (0.34)	11.93 (0.29)	9.85				$3b_{2g}$
e	11.19	11.94 (0.69)	12.02 (0.69)	10.12	10.60	1.60	1.28	$6b_{2u}$
e′	11.35 (sh)	12.23 (0.37)	12.36 (0.33)	10.10				$2b_{1u}$
e″	11.67 (sh)	13.27 (1.72)	13.20 (1.84)	11.21	11.00	0.79	1.01	$8a_g$

[a] The repolarization energy values are reported in parentheses. PT values represent the repolarization contributions (scaled by a 0.75 factor; see text) to the total reorganization energy. [b] Experimental IE's are related to the position of Gaussian components. [c] The intensity of band a has been taken as reference. [d] See Table IV for the dominant character of each MO.

crystal by a network of intermolecular hydrogen bonds.[29] Mass spectra[31] are indicative of monomeric structures in the vapor phase, but no information exists for the conformation adopted. However, the present all-electron ab initio calculations provide an indication that the stability of the trans conformer (C_{2h}) exceeds that of the cis conformer by ca. 7 kcal/mol.[32]

The electronic structure of Hgly can be qualitatively described in terms of two interacting formaldoxime subunits. The latter molecule is an electron-rich system, the more external MO's of which consist of the in-plane N_{2p} lone pair and of two out-of-plane π MO's (a π C=N and a lone-pair orbital that is primarily O_{2p} in character).[33] The in-phase and out-of-phase combinations of these uppermost MO's in the appropriate point group together with a C–C σ orbital describe adequately the seven uppermost MO's in Hgly. Among the four π MO's (π_{1-4}), two represent combinations of O_{2p} lone pairs while the remainder are typical of a conjugated diene system (Figure 2). Finally, the two σ MO's can be described in terms of combinations of N_{2p} lone pairs (n_+ and n_-) (Figure 2).

A detailed analysis of the Hgly MO's emerges from PSHONDO population data[34] compiled in Table I for both the cis and trans conformers. The compositions of the seven uppermost MO's agree well with the aforementioned qualitative analysis. The lower energy orbitals that follow, starting from $5b_1$, represent σ systems

(31) The mass spectra were recorded with a KRATOS MS 50 spectrometer.
(32) In the absence of a full geometry optimization, this numerical result should be viewed as approximate.
(33) Liotard, D.; Dargelos, A.; Chillet, M. *Theor. Chim. Acta* **1973**, *31*, 325.
(34) Identical results (within 1%) are obtained by an all-electron ab initio calculation using the 4-31G basis set within a GAUSSIAN 80 code.

Table VII. PSHONDO Eigenvalues and Population Analysis of Outermost MO's of $Pt(gly)_2$

MO	eigenvalue, eV	% population								overlap pop. Pt–N	dominant character
		Pt									
		5d	6s	6p	N	C	O	H	H′		
$3b_{3g}$	−9.82	12			30	26	32			−0.054	π_4, d_{yz}
$2a_u$	−10.12				28	21	51			0.000	π_4
$9a_g$	−11.35	64	25		5		5	1		0.020	d_{z^2}, 6s
$7b_{3u}$	−11.72			1	15	4	80			0.012	n_+
$3b_{2g}$	−11.78	31			3	44	22			−0.022	π_3, d_{xz}
$6b_{1g}$	−12.54	7			2	2	88	1		−0.004	n_-
$2b_{1u}$	−12.71				3	34	63			0.000	π_3
$6b_{2u}$	−13.13			1	48	4	41	3	3	0.010	n_-
$2b_{3g}$	−13.20	71					29			0.000	d_{yz}, π_2
$2b_{2g}$	−13.34	47				1	52			0.000	d_{xz}, π_3
$8a_g$	−13.78	68	1		4	2	24	1		−0.030	$d_{x^2-y^2}$, d_{z^2}, σ
$6b_{3u}$	−14.70			1	33	26	30	10		0.010	σ
$7a_g$	−16.11	39	1		10	12	26	6	6	0.066	σ, $d_{x^2-y^2}$, d_{z^2}
$1a_u$	−16.44				46	8	46			0.000	π_2
$6a_g$	−16.88	1			6	42	33	8	10	−0.002	σ
$1b_{3g}$	−17.32	16			43	6	35			0.035	π_2, d_{yz}
$5b_{1g}$	−17.42	9			37	2	51	1		0.004	σ, d_{xy}
$1b_{1u}$	−17.74			1	48	23	28			0.004	π_1
$1b_{2g}$	−18.24	17			46	21	16			0.038	π_1, d_{xz}
$5b_{2u}$	−18.34				26	30	24	20		0.000	σ

Table VIII. Relevant PE Data, Computed IE's, and Assignments of the PE Spectra of $Pt(gly)_2$ and $Pt(dmg)_2$

band label	$Pt(gly)_2$ IE, eV			$Pt(gly)_2$ rel intens[c]		$Pt(dmg)_2$ IE, eV	assignt[d]
	exptl[a]	ΔSCF[b]	PT[b]	He I	He II		
a′	8.36	9.29 (2.06)	9.02 (2.43)	0.78	1.19	7.87 (sh)	$9a_g$
a	8.77	9.40 (0.42) 9.72 (0.40)	9.56 (0.40) 9.90 (0.35)	2.00	2.00	8.20	$3b_{3g}$ $2a_u$
b	9.59	10.93 (0.79)	11.05 (0.76)	0.69	0.69	8.94	$7b_{3u}$
c	10.02	11.16 (0.98) 11.40 (1.80)	11.28 (0.61) 11.15 (2.11)	1.87	2.48	9.24	$3b_{2g}$ $2b_{3g}$
d	10.70		11.71 (2.17)	1.02	1.20	10.06	$8a_g$
e	11.28		11.75 (0.91) 12.30 (1.09)	2.03	2.33	10.63	$6b_{1g}$ $2b_{2g}$
e′	11.80		12.47 (0.33) 12.55 (0.65)	1.60	1.20	11.10 (sh)	$2b_{1u}$ $6b_{2u}$

[a] Experimental IE's are related to the position of Gaussian components. [b] The repolarization energy values are reported in parentheses. PT values represent the repolarization contributions (scaled by a 0.75 factor; see text) to the total reorganization energy. [c] The intensity of band a has been taken as reference. [d] See Table VII for the dominant character of each MO.

delocalized over the entire molecular framework (Figure 2). No significant differences are found in the two conformers as far as the most relevant PSHONDO MO composition, orbital, and overlap population data are concerned. Some differences are, in contrast, observed in the sequence of eigenvalues associated with the aforementioned MO's (Figure 2). In particular, the n_- and n_+ combinations are almost accidentally degenerate in the trans conformer because of the operation of a through-bond[35] interaction mechanism involving more internal σ MO's, while they are well separated in the cis conformation because of a 0.53-eV upward energy shift of the n_- component. The predominance of a through-space[35] interaction mechanism is likely responsible for this effect in the cis conformation.

The PE spectrum of Hgly is shown in Figure 3. It consists of three well-resolved bands (a–c) in the region up to 13 eV. A less resolved band system, probably consisting of four bands, follows up to 17 eV. PT PSHONDO and ΔSCF IE's are compared with experimental values in Figure 2 and Table II. A satisfactory fitting of the experimental data is observed, and the assignments that emerge appear to be in good agreement with literature data on formaldoxime.[36]

On passing to spectra of Hdmg, we note, in accordance with relative intensity data (Table II), that bands b and c coalesce into a single structure because of a differential upward IE shift of the two bands. In particular, band c suffers a 0.98-eV shift whereas a +0.3–0.4-eV shift is associated with the remaining a and b bands. The preferential "substituent effect" on the MO's having a significant amplitudes on the carbon atoms α to the methyl groups accounts well for this observation.[37]

Glyoximate Complexes. Bis(glyoximate) complexes of d^8 transition-metal ions have isomorphous square-planar crystal structures[6,30] significantly stabilized by symmetrical hydrogen bonds (Figure 1). Deviations from coplanarity of chelated rings are sometimes observed in the Ni complexes because of close intermolecular contacts.[38] These interactions, peculiar to the solid-state structures, should not exist in the vapor phase. Here, a planar D_{2h} molecular structure can be safely assumed.

An accurate description of perturbations upon the ligand electronic system due to complex formation requires the full understanding of effects due to deprotonation, to charge redistribution, and, finally, to interactions with relevant metal orbitals.

Table III lists the population analyses of the upper filled MO's of the ligand cluster $(gly)_2^{2-}$. As expected, they consist of in-phase

(35) Hoffmann, R. *Acc. Chem. Res.* **1971**, *4*, 2294.
(36) Sandorfy, C.; Dargelos, A. *J. Chem. Phys.* **1977**, *67*, 3011.
(37) Libit, L.; Hoffmann, R. *J. Am. Chem. Soc.* **1974**, *96*, 1370.
(38) Holm, R. H.; O'Connor, M. J. *Prog. Inorg. Chem.* **1971**, *14*, 241.
(39) (a) See for example: Berkowitz, J. *Photoabsorption, Photoionization, and Photoelectron Spectroscopy*; Academic: New York, 1979. (b) Gelius, U. In *Electron Spectroscopy*; North-Holland: Amsterdam, 1982; p 311. (c) Louwen, J. N.; Hengelmolen, R.; Grove, D. M.; Oskam, A.; Dekock, R. L. *Organometallics*, **1984**, *3*, 908 and references therein.

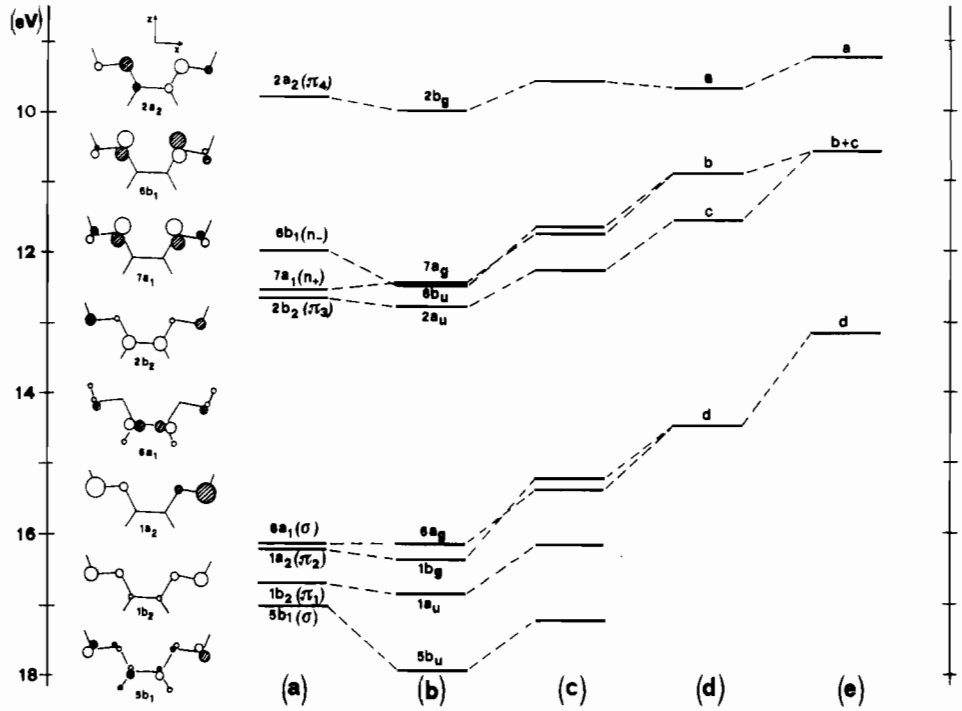

Figure 2. Correlation diagram between Koopmans' eigenvalues of Hgly in the cis (a) and trans (b) conformations, PT IE's of *trans*-Hgly (c), and experimental IE's of Hgly (d) and Hdmg (e).

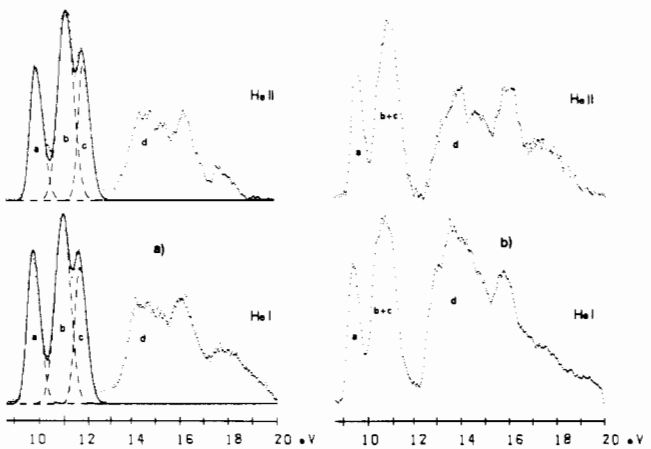

Figure 3. He I and He II PE spectra of Hgly (a) and Hdmg (b): experimental spectrum (point lines); Gaussian components (dashed lines); convolution of Gaussian (solid line).

and out-of-phase combinations of MO's of the two $(gly)^-$ subunits. Of course, the energy splitting between each pair of combinations depends mostly upon Coulombic interligand repulsion terms and, in the case of the n_+ components ($7b_{3u}$ and $7a_g$), is large enough to upset (Figure 4) the energy sequence of the uppermost filled MO's found in the free ligand Hgly. Moreover, the population data give an indication of a greater delocalization in the $(gly)_2^{2-}$ cluster of the macrocyclic H-bonded structure than in the free Hgly ligand.

The effects due to charge redistribution, aside from those due to metal perturbations, upon the complex formation can be analyzed by comparing population data for the $(gly)_2^{2-}$ and $(gly)_2$ clusters since the gross charge delocalized over the ligand macrocycle system is around −0.5 eu in the present complexes (vide infra). The data in Table III give an indication of comparable populations of the various MO's in both cases. Significant differences are found only in the C–N overlap population values. In particular, greater π-population values are associated in $(gly)_2$ with lower σ overlaps. This observation parallels a generalized charge drainage from the $(gly)_2$ ligand σ framework as documented by the lower p_σ orbital population values associated with the O and, to minor extent, C and N atoms (Table III). The

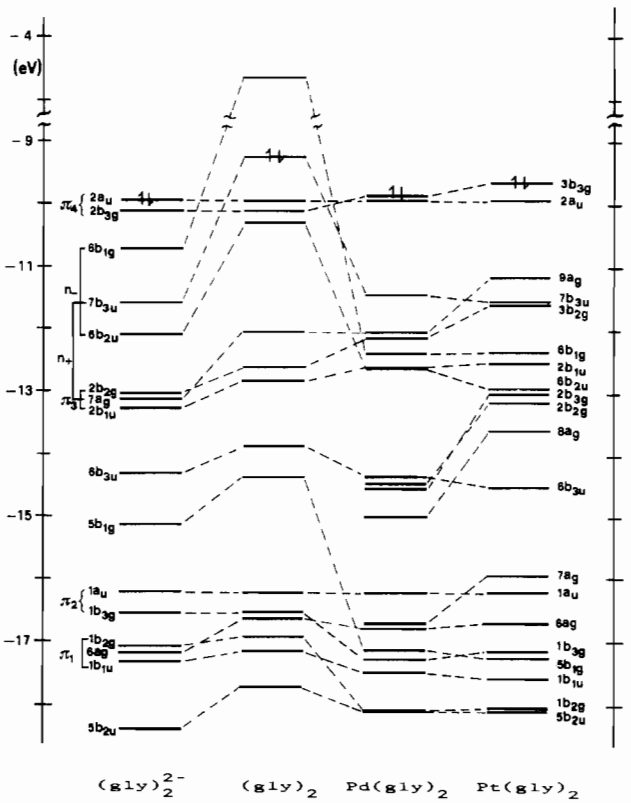

Figure 4. Correlation diagram between the ground-state eigenvalues of $(gly)_2^{2-}$, $(gly)_2$, $Pd(gly)_2$, and $Pt(gly)_2$. The energy scales of $(gly)_2^{2-}$, $(gly)_2$, and $Pt(gly)_2$ are shifted −9.92, +0.18, and +0.21 eV, respectively, relative to those of $Pd(gly)_2$.

overall result is a general destabilization of all NO σ orbitals, thus rendering the $6b_{1g}$ MO the LUMO in $(gly)_2$ (Figure 4).

The interaction with the Pd atom results in severe perturbations of the ligand electronic system. The results of both PSHONDO and Xα–DVM ground-state calculations for $Pd(gly)_2$ are compiled in Tables IV and V. In comparing these results, we note only minor inversions in the energy sequences of some eigenvalues that are grouped within very narrow (~0.2 eV) energy ranges. Im-

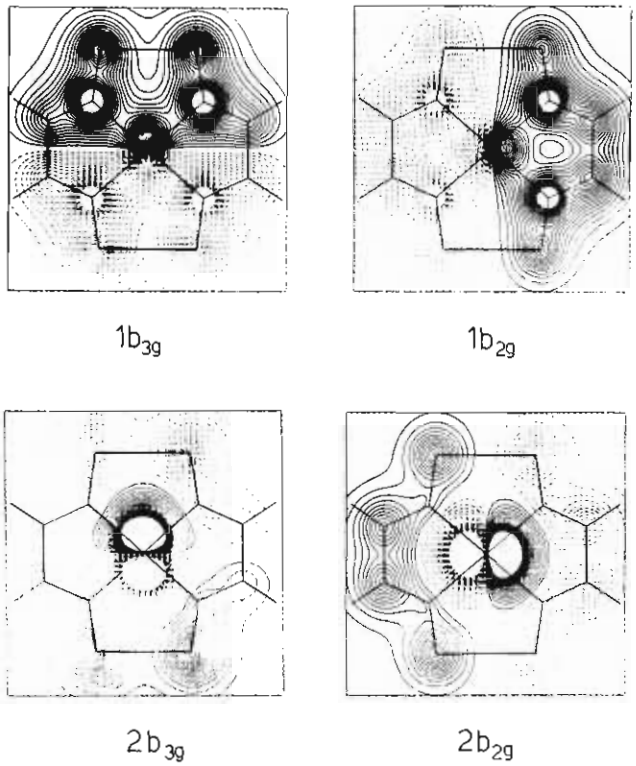

Figure 5. Contour plots of the $Pd(gly)_2$ $1b_{3g}$, $1b_{2g}$, $2b_{3g}$, and $2b_{2g}$ MO's 1.0 au above the $Pd(gly)_2$ molecular plane. The inner blank areas correspond to regions of high electron density. The interval between successive contours is 0.039 $e^{1/2}/Å^{3/2}$.

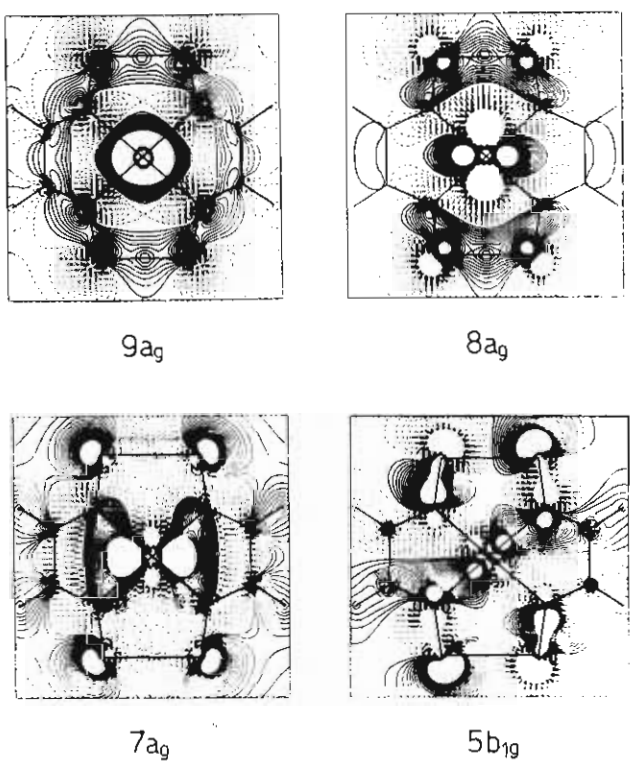

Figure 6. Contour plots of the $Pd(gly)_2$ $5b_{1g}$, $7a_g$, $8a_g$, and $9a_g$ MO's in the $Pd(gly)_2$ molecular plane. The inner blank areas correspond to regions of high electron density. The interval between successive contours is 0.039 $e^{1/2}/Å^{3/2}$.

portantly, MO compositions are almost identical in the Xα and ab initio results. There is indication of major admixture of the metal subshells with a large fraction of the ligand MO's up to 18 eV. Nevertheless, contour diagrams in Figure 5 clearly show that $2b_{2g}$ and $2b_{3g}$ MO's can be described in "classical" terms as

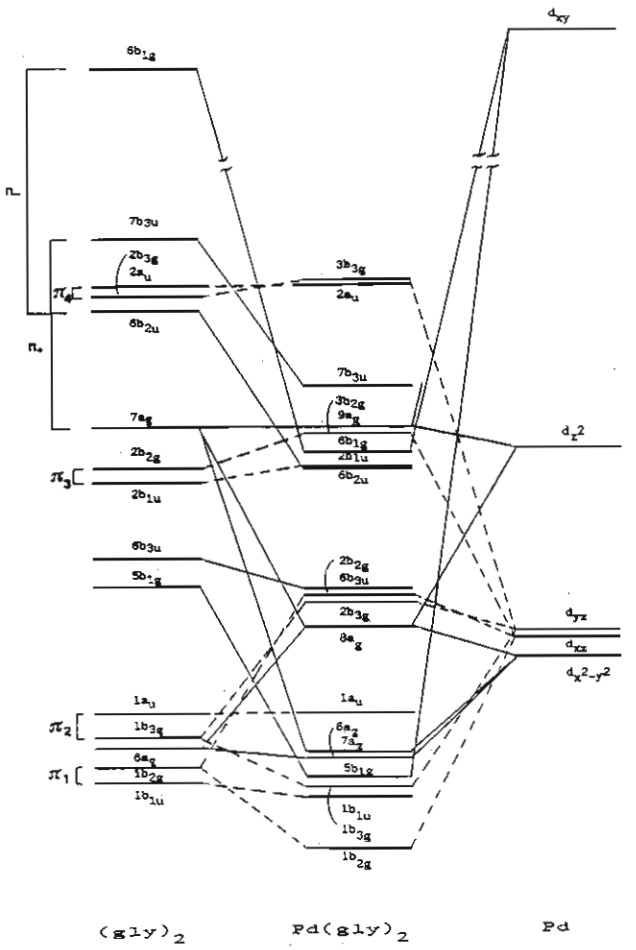

Figure 7. Molecular orbital scheme for $Pd(gly)_2$. σ and π interactions are shown by solid and dashed lines, respectively.

almost pure metal d_{xz} and d_{yz} orbitals. Within this picture, they represent the antibonding counterparts of the strongly bonding $1b_{2g}$ and $1b_{3g}$ MO's (Figure 5), which in turn are the major contributors to the metal–ligand π bonding. Furthermore, the $9a_g$ and $8a_g$ MO's (Figure 6) represent metal d_{z^2} and $d_{x^2-y^2}$ orbitals. Interestingly, both $4d_{z^2}$ and 5s orbitals are significantly admixed into the $9a_g$ MO (Figure 6). As in the case of metal orbitals of π symmetry, the $8\text{–}9a_g$ MO's have antibonding character because of relevant interactions mainly with the $7a_g$ MO (Figure 6), which, of course, is among the MO's largely responsible for the metal–ligand σ bonds. Finally, the contour diagram in Figure 6 reveals unambiguously that the $5b_{1g}$ MO is mostly responsible for bonding interactions with the metal $4d_{xy}$ orbitals. This peculiarity, not found in the case of the $6b_{1g}$ MO, which remains an almost pure O_{2p} lone pair, is certainly due, besides the different MO compositions, to a particular spatial density distribution that, despite a less favorable energy matching, allows better overlap with the metal $4d_{xy}$ orbital.

The details of the metal–ligand bonding can be better described in terms of a qualitative interaction scheme (Figure 7) in which the energies of the $(gly)_2$ MO's have been scaled in order to line up the energy of the $1a_u$ MO with that of the corresponding MO in $Pd(gly)_2$. This MO represents, in fact, a convenient reference since, by symmetry, it cannot interact with any of the metal valence AO's, its energy being only affected by charge redistribution. In this context it is worth noting that the energy separation between the $2a_u$ and $1a_u$ MO's remains constant on going from $(gly)_2^{2-}$ to $Pt(gly)_2$ (Figure 4).

The analysis of the correlation diagram provides information on the nature of the metal–ligand bonding. A very substantial stabilization of all the LB MO's of σ symmetry is noted, which, in the case of the $6b_{1g}$ MO, causes the MO to become filled on passing to the metal complex. We note in passing that these interactions can be described, within a classical ligand field model,

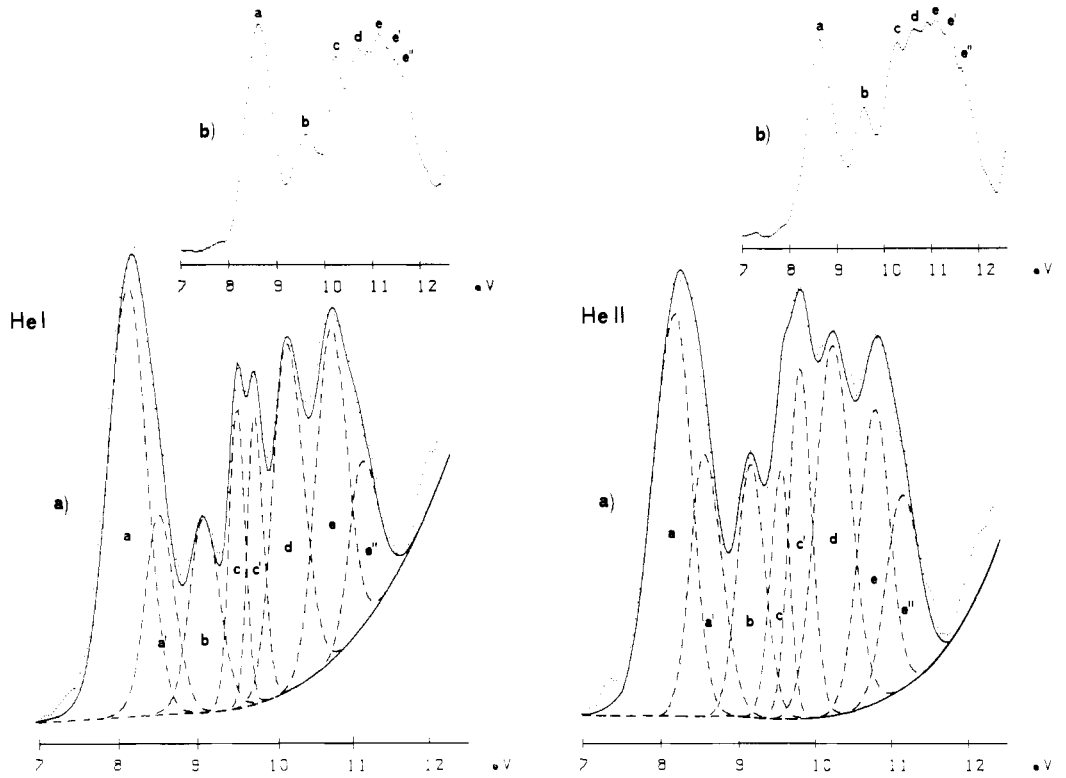

Figure 8. He I and He II PE spectra of $Pd(dmg)_2$ (a) and $Pd(gly)_2$ (b) in the low-IE region: experimental spectrum (point lines); Gaussian components (dashed lines); convolution of Gaussian (solid line).

in terms of σ donation from the $(gly)_2^{2-}$ ligand anion to the Pd^{2+} ion in accordance with atomic charge data (Table V) in the complex. Of particular interest are the metal–ligand interactions among the orbitals of a_g symmetry. The resulting $9a_g$–$6a_g$ MO's provide an important contribution to the Pd–N σ bonding since the $9a_g$ and the $8a_g$, which formally are the antibonding counterparts of the remaining $7a_g$ and $6a_g$ orbitals, acquire a bonding character because of the interactions with the 5s and the $4d_{z^2}$ metal subshells, respectively (Figure 7).

The interactions among orbitals of π symmetry present a more intriguing situation. They involve only filled LB and MB orbitals, the latter lying intermediate in energy between the π_{1-4}-related MO's. Therefore, although most of them provide important Pd–N overlap populations, the total π population vanishes because the positive contributions due to the bonding MO's are cancelled by those of their antibonding partners (Table V).

The PE spectra of $Pd(gly)_2$ and $Pd(dmg)_2$ complexes (Figure 8) are similar and in the region below 11 eV consist of a system of five bands (a–e) that are better resolved in the case of the $Pd(dmg)_2$ spectrum. In the higher IE region, spectra of both compounds show unresolved structures typical of ionization of inner σ MO's, which, in turn, are of minor relevance as far as the metal–ligand bonding is concerned. The relevant IE's are listed in Table VI. Inspection of IE values provides indication of an almost uniform $\sim$+0.6 eV shift on passing from $Pd(gly)_2$ to $Pd(dmg)_2$. Furthermore, band c appears split into components c and c′ while structures d–e show better resolution. Deconvolution of spectral profiles has been performed only for the $Pd(dmg)_2$ spectrum because of its better resolution. Relative intensity data listed in Table VI are normalized to the intensity of the a band, which represents the ionization of $3b_{3g} + 2a_u$ MO's (vide infra) having no metal contribution (Table IV). Significant variations in relative intensities are observed upon switching to He II excitation. In particular, bands a′, c′, d, and e″ become more intense (Table VI).

The comparison of experimental IE, ΔSCF, and Xα–TSIE values (Table VI) clearly shows that better agreement is found between experimental IE's and the theoretical data once reorganization effects in the ion states are taken into account. In particular, both ΔSCF and TSIE values satisfactorily reproduce experimental IE data even though ΔSCF values seem to provide a more reliable rationale for the experimental IE grouping. Nevertheless, it quickly becomes evident that although there is no doubt about the nature of the 11 more external ionizations, the simple comparison of experimental and theoretical IE's cannot provide an unambiguous indication of whether the Xα or the ΔSCF values would better fit the sequence of the uppermost eleven ionizations.

Previous experience shows, however, that the reexamination of theoretical data in the light of additional experimental evidence may be conclusive as far as the assignment of PE spectra is concerned. In particular, we first observe that the total intensity ratio (Table VI) between the band envelope a–b and the remaining structures up to 11 eV is indicative of an occupancy ratio between the corresponding MO's of nearly 8:14 and this, in turn, means an approximately 4:7 ratio between the MO's responsible for the ionization events. Second, the relative intensity data show that bands a′, c′, d, and e″ increase, though moderately, upon switching to the He II ionizing source. The rigorous quantitative evaluation of molecular cross-section variations with the energy of incident radiation remains an unsolved problem due to the poorly understood interplay of a number of effects.[37a] Nevertheless, empirical correlations between relative intensity variations in He I/He II spectral features and the compositions of MO's undergoing ionization have proven entremely useful, especially in the case of strongly localized MO's.[37b] Thus, ionizations from orbitals having a large metal d character are generally characterized by a strong enhancement in intensity upon switching from He I to He II excitation.[8,37c] Therefore, the present behavior is indicative of sizable metal contributions to the corresponding MO's as is the case of $9a_g$, $2b_{2g}$, $2b_{3g}$, and $8a_g$ MO's (Table IV). Finally, we note that band e′ suffers a differential +0.75-eV IE shift with respect to the other bands on passing from $Pd(gly)_2$ to $Pd(dmg)_2$ (Table VI), and we have already recognized that such a behavior can be safely associated with ionizations from MO's of π symmetry having significant *C*-enaminic amplitudes, as is the case of $3b_{2g}$ and $2b_{1u}$ MO's. Given these criteria, the assignment of the spectra of $Pd(gly)_2$ and $Pd(dmg)_2$ becomes a straightforward matter (Table VI). Band a is taken to represent three ionization events, and its components a and a′ (which are clearly resolved in the

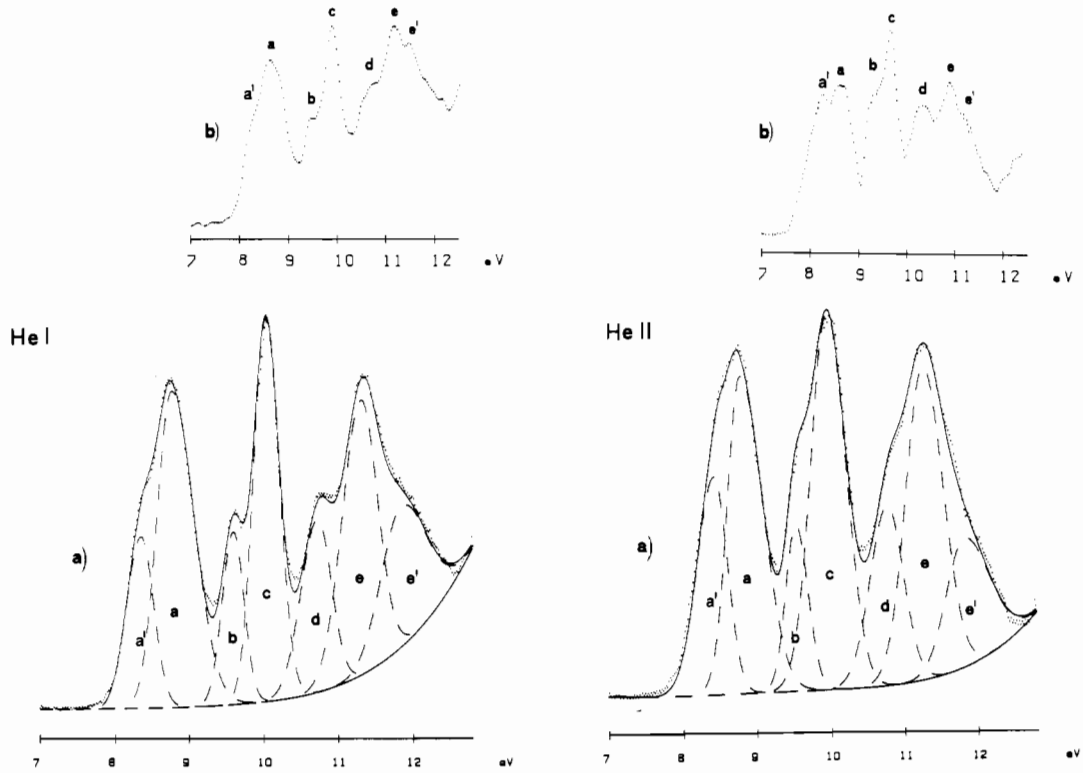

Figure 9. He I and He II PE spectra of $Pt(gly)_2$ (a) and $Pt(dmg)_2$ (b) in the low-IE region: experimental spectrum (point lines); Gaussian components (dashed lines); convolution of Gaussian (solid line).

case of spectra of Pt complexes, vide infra) are assigned to $3b_{3g}$ (π_4) + $2a_u$ (π_4) and to the $9a_g$ MO's, respectively. This latter assignment is in accord both with the ΔSCF IE sequence and the observed higher relative intensity of band a′ in the He II spectrum. Nevertheless, it implies a 40% underestimation of repolarization energies by the ΔSCF ab initio method. By the same token, we assign bands c′, d, and e″ to ionizations of $2b_{2g}$, $2b_{3g}$, and $8a_g$ MO's, respectively. These MO's all possess remarkable Pd 4d contributions, and the aforementioned bands increase in intensity upon switching to the He II spectrum (Table VI). We note in passing that, within these assignments, the energies associated with ΔSCF failures in predicting experimental ionization energies of all the 4d MB MO's are strictly proportional to the metal d percentages in the corresponding eigenvectors (Table IV). The remaining bands, b, c, e, and e′, are assigned respectively to ionizations of the $7b_{3u}$, $6b_{1g}$, $6b_{2u}$, and $2b_{1u}$ MO's in accordance with the ΔSCF values since differential effects are no longer expected for ionization of MO's having no metal d character.

Turning to $Pt(gly)_2$, we note close similarities of atomic populations of MO's having no metal contributions with those of the Pd analogue. In contrast, differences are found in the case of those MO's that are admixed with metal orbitals of a_g, b_{2g}, and b_{3g} symmetry (Table VII). In particular, metal d orbitals of π symmetry, d_{xz} (b_{2g}) and d_{yz} (b_{3g}), appear uniformly distributed among almost all the $Pt(gly)_2$ LB MO's of suitable symmetry whereas, in the case of the Pd complex, sizable admixtures are found only in the $1b_{2g}$ (π_1) and $1b_{3g}$ (π_1) MO's.[40] Furthermore, the $Pt(gly)_2$ metal d_{z^2} and $d_{x^2-y^2}$ orbitals show preferential interactions with the highest lying $9a_g$ and $8a_g$ MO's while, in the Pd complex, they are almost uniformly admixed into the $6a_g$–$9a_g$ orbitals.

These peculiarities result in remarkable differences in the M–N bonding character of the a_g orbitals (Table VII) as well as in the energy sequence of upper filled MO's (Figure 4). The correlation diagram in Figure 4 shows that all the MO's having pronounced ligand character (of course they are of u symmetry) become somewhat stabilized on passing to $Pt(gly)_2$, while the remainder are subjected to an almost generalized upward energy shift. The effect appears to be of the same relevance both for the orbitals which can be formally described in terms of almost purely MB orbitals ($8a_g$ ($d_{x^2-y^2}$), $9a_g$ (d_{z^2}), and $2b_{3g}$ (d_{yz})) as well as for the higher lying LB MO's significantly admixed with them.

An adequate rationale for these observations can be proposed in terms both of an upward (relative to Pd) energy shift of the unperturbed Pt 5d atomic orbitals and of a greater ligand-to-metal charge transfer to metal 6s virtual orbitals that finally reduces both the negative charge on the ligand framework and, in turn, the positive charge borne by the central metal atom (Table V).

The PE spectra of the Pt complexes, although resembling those of Pd analogues, appear much better structured (Figure 9). Table VIII lists experimental as well as computed IE's. A more satisfactory agreement is found than in the case of $Pd(gly)_2$. The band envelope a, which is now clearly resolved into two components, is assigned to the $9a_g^{-1}$ (a′) and to the $3b_{2g}^{-1}$ + $2a_u^{-1}$ (a) ionizations. The growth of the a′ component in the He II spectrum agrees well with the high Pt 5d character in the corresponding orbitals. Next, band b, the intensity of which remains constant on changing the ionizing source, is assigned to the ionization from the LB $7b_{3u}$ MO. Band c is taken to represent the ionization from $2b_{3g}$ and $3b_{2g}$ MO's. Both these MO's possess relevant metal d contributions in accordance with the greater relative band intensity in the He II spectrum. Despite computed IE values (Table VIII) giving an indication of two almost coincident ionization events ($6b_{1g}^{-1}$ and $8a_g^{-1}$), band d has a relative intensity clearly indicative of a single ionization. Since the band intensity increases in the He II spectrum, this latter feature is assigned to the ionization of the $8a_g$ MO. Similarly, intensity arguments (both in the He I spectrum alone as well as in comparative He I vs He II spectra) suggest the assignment of the adjacent band e to the two $6b_{1g}^{-1}$ and $2b_{2g}^{-1}$ ionizations. Finally, we assign the last band e′ to the remaining LB $2b_{1u}^{-1}$ and $6b_{2u}^{-1}$ ionizations.

Conclusions

This work reinforces our earlier contention that correlated experimental and theoretical studies on selected series of square-planar complexes with chelating bidentate ligands are a unique way to probe their electronic structures and, in turn, the details of the metal–ligand bonding. It is becoming clear, in fact, that models which consider the complex formation in terms of

(40) Note that, as a consequence, $d_{xz,yz}(2b_{2g})$, $(2b_{3g})$ orbitals have nonbonding character in $Pt(gly)_2$ but a slightly antibonding nature in $Pd(gly)_2$.

simple perturbations on the metal electronic system cannot account for the spectroscopic properties of these classes of complexes as well as for their low-dimensional crystal structures and collective solid-state properties.

In particular, both ab initio pseudopotential and first-principles local-exchange DV–Xα calculations combined with He I/He II photoelectron spectroscopic measurements provide convincing descriptions of the metal–ligand bonding. The leading information that emerges from the present study (see also part 1 of the series in ref 8) is that the peculiarities of the ligand electronic system are of major relevance in stabilizing complex formation. These include σ MO's, which can be formally described in terms of symmetry combinations of in-plane lone pairs of ligand heteroatoms (they closely resemble the σ metal–ligand orbitals in systems with so-called "purely σ-donor ligands") as well as more internal systems delocalized over the entire σ framework. Both are equally involved in the metal–ligand bonding and are responsible for a massive ligand-to-metal charge transfer involving empty nd_{xy} and $(n + 1)$s metal orbitals. We note in passing that the transfer involving the more internal ligand orbital of a_g symmetry is mediated by an extensive admixture of d_{z^2}, $d_{x^2-y^2}$, and s metal subshells that, in contrast to the case of D_{4h} complexes, is allowed in D_{2h} symmetry. The description of interactions involving the π systems is much more intriguing since it involves four MO's, the energy matching of which with metal d subshells, critically depends on the nature of the metal atom. In the Pd complexes, interactions with more internal π_1 and π_2 are predominant over those with π_3 and π_4 orbitals and, therefore, raise (more than lower) the energies of unperturbed metal $d_{xz,yz}$ subshells. Thus, the present glyoximates behave as strong σ,π-donor, weak π-acceptor ligands.

In the Pt complexes, a greater σ electron density transfer to the empty 6s metal orbitals is noted that lowers the positive Pt charge. This effect, besides the upward shift expected on passing from Pd to Pt atoms, further raises the energies of metal d subshells, thus also favoring π interactions with more external π_4 and π_3 ligand orbitals.

The energy sequences of the states produced upon ionization are largely dominated by reorganization effects in the ion. Of course, repolarization energies paralleling the metal d-orbital contribution to a particular MO are large enough to upset the energy sequence of ground-state MO's. PT ionization energies are comparable to ΔSCF IE values when taken to 75% of the computed values but do not provide an adequate rationale for the ionization events in the PE spectrum of $Pd(gly)_2$. The same is true even when DV–Xα TSIE's are considered. There is no doubt, however, about the nature of the 11 uppermost ionizations since both ΔSCF and TSIE values provide the same indication. Nevertheless, the experimental criterion based on relative intensity changes upon switching to the He II radiation has proven, once again, to be a powerful tool for establishing the correct ionization sequence.

Finally, we comment on electronic structure related to collective transport properties frequently found in 1-D, partially oxidized bis(glyoximato) complexes of d^8 transition metals. In a simple tight-binding band picture,[7] the properties of the conduction band, which is no longer completely full after partial oxidation, are dictated by the properties of the overlapping monomer HOMO's. Within this picture, both the $3b_{3g}$ and $2a_u$ ground-state MO's of $Pd(gly)_2$ can contribute to the conduction band of the molecular stack. This implies a predominantly ligand-centered π-electron conduction process, analogous to partially oxidized $Ni(gly)_2$[3g] and Ni(Pc) systems.[10,41] However, chemical partial oxidation should induce MO relaxation effects reminiscent of reorganization effects accompanying ionization processes. From Table VI it can be seen that both the $3b_{3g}^{-1}$ and $2a_u^{-1}$ ligand-based ion states as well as the $9a_g^{-1}$ metal-based ion states lie within an energy range comparable to the anticipated[3g,41] bandwidth. Thus, both ligand π-based and metal-based orbitals could play a role in charge transport. In contrast, extrapolation of the present findings to partially oxidized stacked $Pt(gly)_2$ systems suggests charge transport predominantly via the metal chain as in tetracyanoplatinate conductors.[42] These simple models do not, of course, explain the temperature dependence of charge transport[43] in the Pd compounds[3g,5b–d] (the Pt complexes do not form partially oxidized solids upon halogenation). Further experimental characterization of these and new glyoximato systems is in progress.

Acknowledgment. We thank the Consiglio Nazionale delle Ricerche (CNR, Rome, Italy), the Ministero della Pubblica Istruzione (MPI, Rome, Italy), and the U.S. Office of Naval Research for financial support. This research was in part also supported by the NATO Research Grants Program (Grant 068/84 to I.F. and T.J.M.).

Registry No. Hgly, 557-30-2; Hdmg, 95-45-4; gly^-, 44427-82-9; gly, 6918-13-4; $Pd(gly)_2$, 14408-64-1; $Pt(gly)_2$, 26673-00-7; $Pd(dmg)_2$, 14740-97-7; $Pt(dmg)_2$, 17632-92-7.

(41) (a) Almeida, M.; Kanatzidis, M. G.; Tonge, L. M.; Marks, T. J.; Marcy, H. O.; McCarthy, W. J.; Kannewurf, C. R. *Solid State Commun.* **1987**, *63*, 457. (b) Gaudiello, J. G.; Marcy, H. O.; McCarthy, W. J.; Moguel, M. K.; Kannewurf, C. R.; Marks, T. J. *Synth. Met.* **1986**, *15*, 115. (c) Inabe, T.; Nakamura, S.; Liang, W.-B.; Marks, T. J.; Burton, R. L.; Kannewurf, C. R.; Imaeda, K. I. *J. Am. Chem. Soc.* **1985**, *107*, 7224. (d) Inabe, T.; Marks, T. J.; Burton, R. L.; Lyding, J. W.; McCarthy, W. J.; Kannewurf, C. R.; Reisner, G. M.; Herbstein, F. H. *Solid State Commun.* **1985**, *54*, 501.

(42) Williams, J. M.; Schultz, A. J.; Underhill, A. E.; Carneiro, K. In *Extended Linear Chain Compounds*; Miller, J. S., Ed.; Plenum: New York, 1982. Vol. 1, p 73.

(43) Hale, P. D.; Ratner, M. A. *J. Chem. Phys.* **1985**, *83*, 5277 and references therein.